Construction of low-dissipative high-order well-balanced filter schemes for non-equilibrium flows

By W. Wang, H. C. Yee†, B. Sjögreen‡, T. Magin† and C.-W. Shu¶

1. Motivation and objective

Recent progress in the development of a class of low-dissipative high-order filter schemes for multiscale Navier-Stokes and magnetohydrodynamics (MHD) systems by Yee *et al.* (1999), Sjögreen & Yee (2004) and Yee & Sjögreen (2007) shows good performance in multiscale shock/turbulence simulations. The highly parallelizable high-order filter methods consist of two steps, a full-time step of spatially high-order non-dissipative base scheme and an adaptive multistep filter. The nonlinear filter consists of the products of wavelet-based flow sensors and the dissipative portion of high-order shock-capturing schemes.

In the recent paper by Wang *et al.* (2009), well-balanced finite difference WENO schemes and second-order TVD schemes were studied for chemical non-equilibrium flows, extending the well-balanced finite difference WENO schemes for shallow water equations by Xing & Shu (2005,2006). A well-balanced scheme (LeVeque 1998), which can preserve certain nontrivial steady-state solutions exactly, may help minimize some of the oscillations around steady states. It was also shown in Wang *et al.* (2009) that the well-balanced schemes capture small perturbations of the steady-state solutions with high accuracy. While general schemes can only resolve perturbations at the level of truncation error with the specific grid, well-balanced schemes can resolve much smaller perturbations, usually at 1% or lower of the main steady-state flow.

The objective of this work is to generalize the well-balanced approach for non-equilibrium flow to a class of low-dissipative high-order shock-capturing filter schemes. The idea of designing a well-balanced filter scheme is straightforward, i.e., choosing a well-balanced base scheme with a well-balanced filter (both with high-order). The new filter scheme with the well-balanced property will gather the features of both filter methods and well-balanced properties: It can preserve certain steady-state solutions exactly; it is able to capture small perturbations, e.g., turbulence fluctuations; it adaptively controls numerical dissipation. Thus it shows high accuracy, efficiency and stability in shock/turbulence interaction simulations.

2. Governing equations and physical model

Considering an atmospheric entry flow in chemical non-equilibrium and thermal equilibrium, the thermodynamic properties account for excitation of the electronic states for the atoms and molecules, using the rigid-rotor harmonic-oscillator approximation for the molecules (see Magin *et al.* 2006 and Panesi *et al.* 2009).

† NASA Ames Research Center, Moffett Field, CA 94035
‡ Lawrence Livermore National Laboratory, Livermore, CA 94551
¶ Division of Applied Mathematics, Brown University, Providence, RI 02912

Assuming neither dissipative effects nor radiation, the considered physical model is a system of hyperbolic conservation laws with source terms denoted by

$$U_t + \nabla \cdot F(U) = S(U), \tag{2.1}$$

$$U = \begin{pmatrix} \rho_1 \\ \cdots \\ \rho_{n_s} \\ \rho\mathbf{u} \\ \rho e \end{pmatrix}; \quad F(U) = \begin{pmatrix} \rho_1\mathbf{u} \\ \cdots \\ \rho_{n_s}\mathbf{u} \\ \rho\mathbf{u}\mathbf{u} + pI \\ (\rho e + p)\mathbf{u} \end{pmatrix}; \quad S(U) = \begin{pmatrix} s^1 \\ \cdots \\ s^{n_s} \\ \mathbf{0} \\ 0 \end{pmatrix}; \tag{2.2}$$

where n_s is the number of species; ρ_s, the mass density of species s; $\mathbf{u}$, the velocity vector; and e, the internal energy per unit mass of the mixture. The mixture mass density is defined as $\rho = \sum_{s=1}^{n_s} \rho_s$, and the pressure p is given by the perfect gas law

$$p = RT \sum_{s=1}^{n_s} \frac{\rho_s}{M_s}, \tag{2.3}$$

where R is the universal gas constant, and M_s, the molar mass of species s. The temperature T can be found from the total energy

$$\rho e = \sum_{s=1}^{n_s} \rho_s e_s(T) + \frac{1}{2}\rho|\mathbf{u}|^2, \tag{2.4}$$

where the internal energy e_s of species s is a function of temperature

$$e_s(T) = e_s^T(T) + e_s^E(T) + e_s^F, \quad s \in H_a, \tag{2.5}$$

$$e_s(T) = e_s^T(T) + e_s^E(T) + e_s^R(T) + e_s^V(T) + e_s^F, \quad s \in H_p, \tag{2.6}$$

where H_a is the set of atoms and H_p is the set of molecules. The translational energy of species s is given by

$$e_s^T(T) = \frac{3}{2}\frac{R}{M_s}T, \tag{2.7}$$

and the electronic energy contribution by

$$e_s^E(T) = \frac{R}{M_s}\frac{\sum_n g_{s,n}^E \theta_{s,n}^E \exp\left(\frac{-\theta_{s,n}^E}{T}\right)}{\sum_n g_{s,n}^E \exp\left(\frac{-\theta_{s,n}^E}{T}\right)}, \tag{2.8}$$

where quantities $g_{s,n}^E$ and $\theta_{s,n}^E$ stand for the degeneracy and characteristic temperature of the electronic level n of species s. The number of electronic levels retained is limited for mathematical and physical standpoints. The partition function leading to thermodynamic properties diverges when all levels are accounted for. The maximum number of electronic levels of each atom and molecule is progressively increased up to a correspondence between the values of computed enthalpies and accurate reference tables. For molecule s, the rotational energy is assumed to be described by means of a rigid rotor model

$$e_s^R(T) = \frac{RT}{M_s}, \tag{2.9}$$

and the vibrational energy, by means of a harmonic oscillator model

$$e_s^V(T) = \frac{R}{M_s} \frac{\theta_s^V}{\exp\left(\frac{\theta_s^V}{T}\right) - 1}, \tag{2.10}$$

where the quantity θ_s^V stands for the vibrational characteristic temperature of the diatomic molecule. To account for the energy released in the gas by chemical reactions between the species, a common level from which all the energies are measured is established by using the formation enthalpy e_s^F at 0^oK.

The source term $S(U)$ describes the chemical reactions occurring in gas flows which result in changes in the amount of mass of each chemical species. In the general case there are J reactions of the form

$$\nu'_{1,j}X_1 + \nu'_{2,j}X_2 + \cdots + \nu'_{n_s,j}X_{n_s} \rightleftharpoons \nu''_{1,j}X_1 + \nu''_{2,j}X_2 + \cdots + \nu''_{n_s,j}X_{n_s}, \quad j = 1, \ldots, J, \tag{2.11}$$

where $\nu'_{i,j}$ and $\nu''_{i,j}$ are respectively the stoichiometric coefficients for the reactants and products of species i in the jth reaction. For non-equilibrium chemistry the rate of production of species i due to chemical reaction may be written as

$$s^i = M_i \sum_{j=1}^{J} (\nu''_{i,j} - \nu'_{i,j}) \left[k_{f,j} \prod_{s=1}^{n_s} \left(\frac{\rho_s}{M_s}\right)^{\nu'_{s,j}} - k_{b,j} \prod_{s=1}^{n_s} \left(\frac{\rho_s}{M_s}\right)^{\nu''_{s,j}} \right], \quad i = 1, \ldots, n_s. \tag{2.12}$$

For each reaction j the forward and backward reaction rate coefficients, $k_{f,j}$ and $k_{b,j}$, are assumed to be known functions of temperature. The forward reaction rate coefficient is given by an Arrhenius law. Following microreversibity the backward rate coefficient is obtained from the expression $k_{f,j} = k_{b,j}/K_{e,j}$, where the equilibrium constant for the jth reaction is given by the relation

$$\ln K_{e,j} = -\frac{1}{k_{\mathrm{B}T}} \sum_{s=1}^{n_s} [(\nu''_{s,j} - \nu'_{s,j}) m_s g_s(p_{ref}, T)], \tag{2.13}$$

where the reference pressure $p_{ref} = 1$ Pa. The Gibbs free energy g_s of species s is a function of pressure and temperature

$$g_s(p,T) = g_s^T(p,T) + g_s^E(T), \quad s \in H_a, \tag{2.14}$$

$$g_s(p,T) = g_s^T(p,T) + g_s^E(T) + g_s^R(T) + g_s^V(T), \quad s \in H_p. \tag{2.15}$$

The translational Gibbs free energy is obtained from

$$g_s^T(p,T) = \frac{RT}{M_s} \ln \left[\frac{RT}{N_A p} \left(\frac{2\pi M_s RT}{N_A^2 h_P^2} \right)^{\frac{3}{2}} \right], \tag{2.16}$$

where the symbol h_P stands for Planck's constant, and N_A for Avogadro's number. The electronic Gibbs free energy reads

$$g_s^E(T) = -\frac{RT}{M_s} \ln \left[\sum_n g_{s,n}^E \exp\left(\frac{-\theta_{s,n}^E}{T} \right) \right]. \tag{2.17}$$

For the diatomic molecule s, the rotational Gibbs free energy is

$$g_s^R(T) = -\frac{RT}{M_s} \ln \left(\frac{T}{\theta_s^R \sigma_s} \right), \tag{2.18}$$

where symbol σ_s stands for the steric factor. The vibrational Gibbs free energy is obtained from the relation

$$g_s^V(T) = \frac{RT}{M_s} \ln \left[1 - \exp\left(\frac{-\theta_s^V}{T} \right) \right]. \tag{2.19}$$

3. Description of high-order filter methods

For simplicity, the numerical methods are described for the one-dimensional case. Denote $A = \partial F/\partial U$, the Jacobian matrix of the flux in equation (2.2). The eigenvalues of A are

$$(a^1, \ldots, a^m) = (u, \ldots, u, u + c, u - c), \tag{3.1}$$

where m is the number of components of vector U, $m = n_s+2$ in the one-dimensional case. c is the frozen speed of sound defined by the expression $c^2 = (\kappa + 1)p/\rho$ with quantity $\kappa = (\sum_{s=1}^{n_s} \rho_s R/M_s)/(\sum_{s=1}^{n_s} \rho_s c_{v,s})$ based on the species-specific heat $c_{v,s} = de_s/dT$. Denote R as the matrix whose columns are eigenvectors of A [not to be confused with the R in equation (2.3)]. Let $a^l_{j+1/2}, R_{j+1/2}$ denote the quantities a^l and R evaluated at some symmetric average of U_j and U_{j+1}, such as Roe's average. Define

$$\alpha_{j+1/2} = R^{-1}_{j+1/2}(U_{j+1} - U_j) \tag{3.2}$$

as the difference of the local characteristic variables in the x direction.

The considered filter method contains two steps, a high-order non-dissipative spatial base scheme step (not involving the use of approximate Riemann solvers or flux limiters) and a multistep filter (usually involving the use of approximate Riemann solvers and flux limiters). The nonlinear filter consists of the product of a wavelet (WAV) sensor and the nonlinear dissipative portion of a high-resolution shock-capturing scheme.

We will briefly review the high-order filter schemes in this section.

3.1. *High-order spatial scheme step*

The first step of the numerical method consists of a time step via a high-order non-dissipative spatial and high-order temporal base scheme operator L^*. After the completion of a full-time step of the base scheme, the solution is denoted by U^*

$$U^* = L^*(U^n), \tag{3.3}$$

where U^n is the numerical solution vector at time level n.

The high-order non-dissipative spatial base schemes could be the standard central schemes or the centered compact scheme.

For strong shock interactions and/or steep gradient flows, a small amount of high-order linear dissipation can be added to the base scheme step to reduce the time step constraint and stability. For example, an eighth-order linear dissipation with the sixth-order central scheme to approximate $F(U)_x$ is written as

$$\frac{\partial F}{\partial x} \approx D_{06}\, F_j + d(\Delta x)^7 (D_+ D_-)^4 U_j, \tag{3.4}$$

where D_{06} is the standard sixth-order accurate centered difference operator, and D_+D_- is the standard second-order accurate centered approximation of the second derivative. The small parameter d is a scaled value (e.g., spectral radius of $A(U)$) in the range of 0.00001-0.0005, depending on the flow problem, and has the sign which gives dissipation in the forward time direction.

3.2. *Adaptive nonlinear filter step (discontinuities and high gradient capturing)*

After the completion of a full-time step of the high-order base scheme, the second step is to adaptively filter the solution by the product of a "wavelet sensor" and the "nonlinear dissipative portion of a high-resolution shock-capturing scheme" (involving the use of flux limiters). The final update step after, e.g., the nonlinear filter step, can be written as

$$U_j^{n+1} = U_j^* - \frac{\Delta t}{\Delta x}\left[H_{j+1/2}^{fx} - H_{j-1/2}^{fx}\right]. \tag{3.5}$$

Here, the filter numerical fluxes

$$H_{j+1/2}^{fx} = R_{j+1/2}\bar{H}_{j+1/2}. \tag{3.6}$$

Denote the elements of the vector $\bar{H}_{j+1/2}$ by $\bar{h}_{j+1/2}^l$, $l = 1, 2, \ldots m$. The nonlinear portion of the filter $\bar{h}_{j+1/2}^l$ has the form

$$\bar{h}_{j+1/2}^l = \frac{1}{2}(s^N)_{j+1/2}^l(\phi_{j+1/2}^l). \tag{3.7}$$

Here, $(s^N)_{j+1/2}^l$ is the sensor to activate the higher-order nonlinear numerical dissipation $\phi_{j+1/2}^l$. $(s^N)_{j+1/2}^l$ is designed to be zero or near zero in regions of smooth flow and near one in regions with discontinuities. $(s^N)_{j+1/2}^l$ varies from one grid point to another and is obtained from a wavelet analysis of the flow solution [see Sjögreen & Yee (2004)]. The wavelet sensor can be obtained from the characteristic variables for each wave or a single sensor for all waves, based on pressure and density. The latter one is used in the report.

The dissipative portion of the nonlinear filter $\phi_{j+1/2}^l = g_{j+1/2}^l - b_{j+1/2}^l$ is the dissipative portion of a high order high-resolution shock-capturing scheme for the local lth characteristic wave. Here $g_{j+1/2}^l$ and $b_{j+1/2}^l$ are numerical fluxes of the uniformly high-order high-resolution scheme and a high-order central scheme for the l-th characteristic wave, respectively.

For the numerical examples, two forms of nonlinear dissipation $\phi_{j+1/2}^l$ were considered, namely:

- The dissipative portion of balanced WENO schemes (see Sec. 4). It is obtained by taking the full WENO scheme and subtracting the central scheme, such as, WENO5-D_{06} and WENO7-D_{08}.
- The dissipative portion of the Harten-Yee TVD scheme (see Yee *et al.* 1999).

4. Description of well-balanced methods

A well-balanced scheme refers to a scheme that preserves exactly specific steady-state solutions of the governing equations. In the previous work by Wang *et al.* (2009), the linear schemes, WENO-Roe scheme, Harten-Yee TVD and the Predictor-Corrector TVD schemes (with zero entropy correction) are proven theoretically and numerically to be well-balanced schemes for the non-equilibrium flow equation (2.1) with zero velocity steady states. We will briefly review the idea of the well-balancedness in this section.

For the general one-dimensional system balance law

$$U_t + F(U, x)_x = S(U, x), \tag{4.1}$$

the steady-state solution U satisfies

$$f^l(U, x)_x = s^l(U, x), \quad l = 1, \ldots, m, \tag{4.2}$$

where f^l and s^l are the lth elements of the vectors $F(U,x)$ and $S(U,x)$.

A linear finite-difference operator D is defined to be one satisfying $D(af_1 + bf_2) = aD(f_1) + bD(f_2)$ for constants a, b and arbitrary grid functions f_1 and f_2. A scheme for equation (4.1) is said to be a linear scheme if all the spatial derivatives are approximated by linear finite-difference operators.

As proved in Xing & Shu 2005, under the following two assumptions regarding equation (4.1) and the steady-state solution of equation (4.2), linear schemes with certain restrictions are well-balanced schemes. Furthermore, high-order nonlinear WENO schemes can be adapted to become well-balanced schemes.

ASSUMPTION 1. *The considered steady-state preserving solution U of equation* (4.2) *satisfies*

$$r_s(U,x) = \textit{constant}, \quad s = 1, 2, \dots \tag{4.3}$$

for a finite number of known functions $r_s(U,x)$.

ASSUMPTION 2. *Each component of the source term vector $S(U,x)$ can be decomposed as*

$$s^l(U,x) = \sum_i \tau_i(r_1(U,x), r_2(U,x), \dots)\, t_i'(x), \quad l = 1, \dots, m, \tag{4.4}$$

for a finite number of functions τ_i and t_i, where τ_i could be arbitrary functions of $r_s(U,x)$, and τ_i and t_i can be different for different $s^l(U,x)$. (Here t_i is not to be confused with the time "t" indicated on all previous conservation laws.)

Now consider the non-equilibrium flow equation (2.1). First, since $S(U,x) \equiv S(U)$, all $t_i'(x) = 1$. Next, when the flow is in the steady state, the chemistry is in equilibrium and thus the source vector $S(U) = 0$. Therefore, the two assumptions are easily satisfied by taking

$$r_i(U) = s^i(U), \quad i = 1, \dots, m. \tag{4.5}$$

Furthermore, linear schemes (such as central schemes) and the WENO-Roe scheme are naturally well balanced for such steady-state solutions of equation (2.1) (see Wang *et al.* 2009).

A well-balanced finite difference WENO-LF scheme can be constructed with a limiter λ in the Lax-Friedrichs flux splitting

$$f^{\pm}(u) = \frac{1}{2}(f(u) \pm \alpha\lambda u). \tag{4.6}$$

λ is close to 0 or 1 according to the solution which is in steady state or away from steady state. In particular, λ is constructed by

$$\begin{aligned} \lambda := \quad & \max\left(\min\left(1, \frac{(|r_1(U_{i+1},x_{i+1}) - r_1(U_i,x_i)| + |r_1(U_{i-1},x_{i-1}) - r_1(U_i,x_i)|)^2}{|r_1(U_{i+1},x_{i+1}) - r_1(U_i,x_i)|^2 + |r_1(U_{i-1},x_{i-1}) - r_1(U_i,x_i)|^2 + \varepsilon}\right),\right. \\ & \left.\min\left(1, \frac{(|r_2(U_{i+1},x_{i+1}) - r_2(U_i,x_i)| + |r_2(U_{i-1},x_{i-1}) - r_2(U_i,x_i)|)^2}{|r_2(U_{i+1},x_{i+1}) - r_2(U_i,x_i)|^2 + |r_2(U_{i-1},x_{i-1}) - r_2(U_i,x_i)|^2 + \varepsilon}\right), \dots\right), \end{aligned} \tag{4.7}$$

where ε is a small number to avoid zero in the denominator and we take it as 10^{-6} in the computations. Near the specific steady state, the differences in r_i shown in (4.7) are close to zero. λ will be near zero when all these differences are small compared with ε. λ is near one if the solution is far from the steady state, since the differences in r_i shown in (4.7) are now on the level of $O(\Delta x)$ and much larger than ε, and then the scheme is the regular WENO-LF scheme. The limiter does not affect the high-order accuracy of the scheme in the smooth region for general solutions of equation (2.1). In the specific steady

state, since all the r_i are constants, λ becomes zero and then the scheme maintains the exact solutions for such steady state.

We remark that the functions r_i in the limiter (4.7) are used to distinguish the states between steady and unsteady. They are not necessarily the same as in Assumption 1, but they must be a necessary condition for the steady states. For example, in the considered "zero velocity" steady state, zero velocity will imply zero source terms and constant pressure, etc. $u = 0$ is a necessary condition for zero velocity steady state. Thus taking $\lambda := \left(\min\left(1, \frac{(|v(U_{i+1},x_{i+1})|+|v(U_i,x_i)|)^2}{|v(U_{i+1},x_{i+1})|^2+|v(U_i,x_i)|^2+\varepsilon}\right)\right.$ also works in the code implementation.

The dissipative portion of the TVD schemes has the form

$$\phi^l_{j+1/2} = \frac{1}{2}\left[\psi(\nu^l_{j+1/2}) - (\nu^l_{j+1/2})^2\right]\left(\alpha^l_{j+1/2} - \hat{Q}^l_{j+1/2}\right), \tag{4.8}$$

where

$$\nu^l_{j+1/2} = \frac{\Delta t}{\Delta x} a^l_{j+1/2}, \tag{4.9}$$

$a_{j+1/2}$ and $\alpha_{j+1/2}$ are defined in (3.1) and (3.2).

The function $\psi(z)$ is an entropy correction to $|z|$ (see Yee 1989) with

$$\psi(z) = \begin{cases} |z| & |z| \geq \delta_1 \\ (z^2 + \delta_1^2)/2\delta_1 & |z| < \delta_1 \end{cases}, \tag{4.10}$$

where δ_1 is the entropy fix parameter (see Yee *et al.* 1991 for a discussion). $\hat{Q}^l_{j+1/2}$ is an unbiased limiter function which can be

$$\hat{Q}^l_{j+1/2} = \text{minmod}(\alpha^l_{j-1/2}, \alpha^l_{j+1/2}) + \text{minmod}(\alpha^l_{j+1/2}, \alpha^l_{j+3/2}) - \alpha^l_{j+1/2} \tag{4.11}$$

with

$$\text{minmod}(a, b) = \text{sgn}(a) \cdot \max\{0, \min[|a|, b\,\text{sgn}(a)]\}. \tag{4.12}$$

It has been proven in Wang *et al.* 2009 that the zero velocity steady-state solution, $R_{j+1/2}\bar{H}_{j+1/2}$ in equation (3.6) maintains zero and thus can be used as the filter part for the well-balanced filter schemes.

5. High-order well-balanced filter scheme

The construction of high-order well-balanced filter schemes is straightforward. The first step is to choose any well-balanced scheme, such as central scheme (CENx) (here x denotes the number 2, 4, 6 or 8) or any linear scheme as the base scheme. The second step is to choose a well-balanced filter, such as the dissipative portion of the TVD scheme (4.8) or the high-order well-balanced WENO scheme.

Here, we remark that these constructed filter schemes are well balanced, except at the interface between the filtered and non-filtered regions. Because in the interface of these two regions, the numerical fluxes get information from different schemes (the base scheme part and the filter part), the schemes will not be well balanced at those interface cells. This is not a serious concern, since the interface is only a small portion of the whole computational domain. Also, since the filter is turned on only at the shock region, the transition region of the shock is usually far away from the considered zero velocity steady state. Thus, there is no need to require the schemes to be well balanced at the interfaces.

Also note that the linear dissipation part $d(\Delta x)^7(D_+D_-)^4U_j$ in the base scheme (3.4) cannot preserve the steady-state solutions. Similar to LF flux, since there are no assumptions on the density functions, the dissipation $d(\Delta x)^7(D_+D_-)^4U_j$ may produce non-zero

values in the steady states. Here, the same idea of constructing well-balanced WENO-LF schemes is applied, i.e., multiplying a limiter λ (4.7) to the linear dissipation part to turn off the linear dissipation in the steady-state area. Since the linear dissipation is needed only for stability concern before reaching steady state, numerical tests show that turning it off by the limiter λ does not affect the stability of the solution. With the limiter λ, the filter schemes will have no linear dissipation in the steady state and thus will maintain the exact steady-state solutions.

In this report, the considered well-balanced filter schemes are central filter schemes CEN2TVDfi, CEN4WENO5fi, CEN6WENO5fi and CEN8WENO7fi. The time discretization is the second-order implicit explicit Runger-Kutta method.

6. Results

In this section, the gas model for sub-orbital Earth reentries comprising five species N_2, O_2, NO, N, and O is described. Then, different numerical tests of the considered high-order well-balanced filter schemes for one- and two-dimensional reacting flows are performed. The purpose of the first example is to numerically verify that the constructed filter schemes are well balanced by time-marching on a nontrivial steady state. In this test the well-balanced filter schemes will show round-off numerical errors for a specific steady-state solution. The second example is a small perturbation over the steady state. We can observe the well-balanced filter schemes showing their advantage in resolving the perturbations in very coarse meshes.

6.1. *Reaction model*

The air mixture is comprised of five species, N_2, O_2, NO, N, and O, with elemental fractions 79% for nitrogen and 21% for oxygen. The spectroscopic constants used in the computation of the species, thermodynamic properties (θ_s^V, $\theta_{s,n}^E$, θ_s^R, g_s^E are given in Sec. 2) and the formation enthalpies are obtained from Gurvich *et al.* (1989). The chemical mechanism is comprised of three dissociation recombination reactions for molecules

$$N_2 + M \rightleftharpoons 2N + M, \quad \text{(see Park 2001)} \tag{6.1}$$

$$O_2 + M \rightleftharpoons 2O + M, \quad \text{(see Park 2001)} \tag{6.2}$$

$$NO + M \rightleftharpoons N + O + M, \quad \text{(see Park 2003)} \tag{6.3}$$

where M is a catalytic particle (any of the species N_2, O_2, NO, N, and O), and two Zeldovich reactions for NO formation

$$N_2 + O \rightleftharpoons NO + N, \quad \text{(see Bose 1996)} \tag{6.4}$$

$$O_2 + N \rightleftharpoons NO + O, \quad \text{(see Bose 1997).} \tag{6.5}$$

6.2. *One-dimensional numerical results*

6.2.1. *Well-balanced test*

The purpose of the first test problem is to numerically verify the well-balanced property of the proposed filter schemes. The special zero-velocity stationary case with

$$T = 1000 \times (1 + 0.2\sin(\pi x))K, \quad p = 10^5\ N/m^2, \quad u = 0\ m/s, \tag{6.6}$$

is considered. The initial composition is based on the local thermodynamic equilibrium (LTE) assumption. Given equation (6.6) and the source term $S(U) = 0$, each species is uniquely determined.

TABLE 1. L^1 relative errors for temperature by central filter schemes at $t = 0.01$.

N	error	error	error	error
	CEN2TVDfi	CEN4WENO5fi	CEN6WENO5fi	CEN8WENO7fi
50	3.84E-11	3.84E-11	3.79E-11	3.67E-11
100	3.79E-11	3.79E-11	3.68E-11	3.62E-11

equation (6.6) is chosen as the initial condition which is also the exact steady-state solution, and the results are obtained by time-accurate time-marching on the steady state. The computational domain is $[-1, 1]$. The L^1 relative errors of temperature at $t = 0.01$ (about 1000 time steps for $N = 100$ grid points) are listed in Table 1. The L^1 relative error is measured to be the difference between the exact solution equation (6.6) and the numerical solution divided by the L^1 norm of the exact solution.

Table 1 shows that the considered high-order central filter schemes are well balanced because they produce errors at the level of machine round-off errors in double precision.

6.2.2. *Small perturbation*

The following test problem will demonstrate the advantages of well-balanced schemes through the problem of a small perturbation over a stationary state.

The same stationary solution, equation (6.6), is considered. A small perturbation $\epsilon = 10^{-3} \times \sin(\pi x)$ is added to the velocity, i.e.,

$$u' = u + \epsilon. \tag{6.7}$$

The other quantities are kept unperturbed. The velocities computed by central filter schemes at $t = 0.1$ are shown in figure 1. The reference results are computed by WENO-Roe with 1200 points and are considered to be "exact".

The results show that all the considered high-order well-balanced filter schemes can capture the small perturbation well in a very coarse mesh $N = 50$. However, the non well-balanced schemes behave in a very oscillatory fashion, such as WENO-LF, without the limiter λ in (4.7), with 200 points (figure 2). These schemes can only resolve the solution when the mesh is refined enough such that the truncation error of the scheme is much smaller than the perturbation.

6.3. *Two dimensional numerical results*

As mentioned in the beginning, extending the well-balanced schemes to the zero velocity steady state of two-dimensional reacting flow is straightforward because the reacting term does not explicitly depend on the dimensions. In this section, similar well-balanced tests to two-dimensional reacting flow will be performed.

6.3.1. *Two-dimensional Well-balanced test*

Similar to the one-dimensional case, the first example is to check that our scheme maintains the two-dimensional zero velocity steady state exactly. The two-dimensional special stationary case

$$T = 1000 \times (1 + 0.2 \sin(\pi(x + y)))K, \quad p = 10^5\ N/m^2, \quad \mathbf{u} = \mathbf{0}\ m/s, \tag{6.8}$$

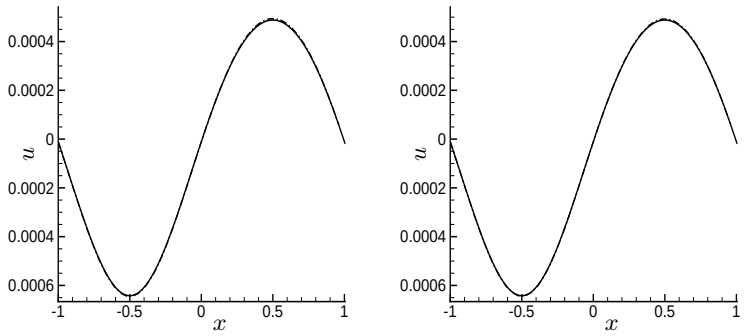

FIGURE 1. Small perturbation of velocity results by central filter schemes: $\epsilon = 10^{-3} \times \sin(\pi x)$. *Left*: CEN6WENO5fi 50 points; *Right*: CEN8WENO7fi 50 points (Central filter schemes: dash–dot; Reference 1200 points: solid).

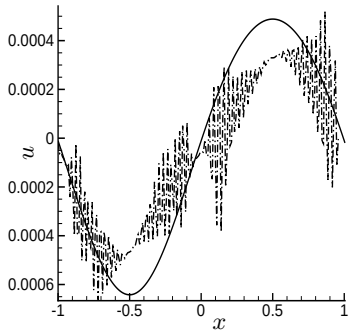

FIGURE 2. Small perturbation of velocity results by WENO-LF scheme: $\epsilon = 10^{-3} \times \sin(\pi x)$. WENO-LF 200 points: dash-dot; Reference 1200 points: solid).

TABLE 2. L^1 relative errors for temperature by central filter schemes at $t = 0.01$.

$N \times N$	error	error	error	error
	CEN2TVDfi	CEN4WENO5fi	CEN6WENO5fi	CEN8WENO7fi
50×50	4.14E-11	4.14E-11	4.21E-11	4.30E-11
100×100	4.04E-11	3.69E-11	3.73E-11	3.82E-11

is considered. The computation is performed to $t = 0.01$ (about 2000 time steps for 100×100 grid points) on the domain $[-1, 1]^2$. Table 2 shows the L^1 relative errors for the temperature T. We can clearly see that the L^1 relative errors are at the level of round-off errors, verifying the well-balancedness of the considered central filter schemes for two-dimensional reacting flow.

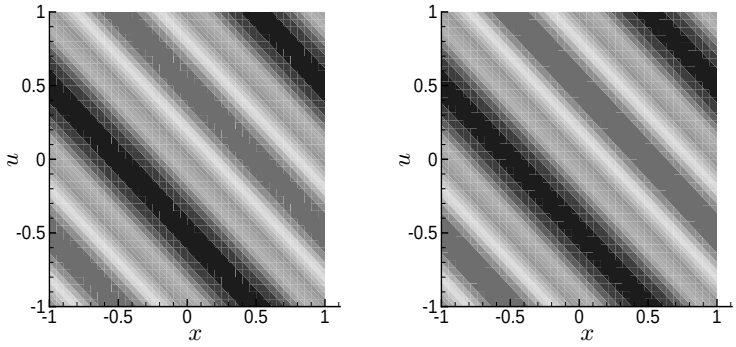

FIGURE 3. Two-dimensional small perturbation of velocity results by central filter schemes: $\epsilon = 10^{-3} \times \sin(\pi(x+y))$. *Left*: CEN6WENO5fi 40×40 points; *right*: CEN8WENO7fi 40×40 points. Contour range: $-0.00024 \sim 0.0001$.

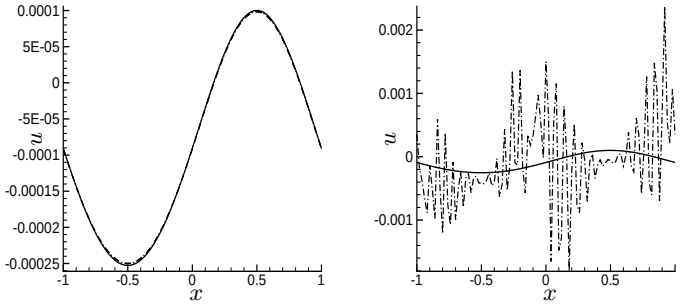

FIGURE 4. Cross section of two-dimensional velocity results at $y = 0$: $\epsilon = 10^{-3} \times \sin(\pi(x+y))$. *Left*: central filter schemes (CEN6WENO5fi: dash-dot; CEN8WENO7fi: dash; Reference: solid); *right*: WENO-LF (WENO-LF: dash-dot; Reference: solid).

6.3.2. *Two-dimensional small perturbation test*

The second example is again a small perturbation test but on a two-dimensional steady state. The same two-dimensional steady-state solution equation (6.8) is considered. A small perturbation $\epsilon = 10^{-3} \times \sin(\pi(x+y))$ is added to the velocity in the x direction, i.e.,

$$u' = u + \epsilon. \tag{6.9}$$

The other quantities are kept unperturbed. The reference solution is computed by the WENO-Roe scheme with 200×200 points. Figure 3 show the contours of velocity by sixth and eighth central filter schemes at $t = 0.01$. The one-dimensional cross-section results by central filter schemes and WENO-LF are shown in figure 4 left and right subplots separately. We can see that our well-balanced filter schemes can capture the small perturbation in a coarse mesh 40×40 very well. However, the WENO-LF produces large oscillations even in a mesh 100×100 (right subplots of figure 4).

7. Future plans

In this report the well-balanced approach is extended to the high-order central filter schemes in solving the reacting flow with five species in one- and two-space dimensions. Numerical examples are given to demonstrate the well-balanced property, accuracy, and good capturing of the small perturbation of the steady-state solutions, and the non-oscillatory shock resolution of the proposed well-balanced filter schemes. Future research will consider the non-zero velocity steady state and the advantages of well-balanced schemes to various steady-state problems.

Acknowledgments

The authors acknowledge the support of the DOE/SciDAC grant. The work by Bjorn Sjögreen was performed under the auspices of the U.S. Department of Energy at Lawrence Livermore National Laboratory under Contract DE-AC52-07NA27344, LLNL-JRNL-420355.

REFERENCES

Bose, D. & Candler, G.V. 1996 Thermal rate constants of the N_2+O→ NO+N reaction using ab initio $^3A''$ and $^3A'$ potential energy surfaces *J. Chem. Phys.* **104**, 2825–2833.

Bose, D. & Candler, G.V. 1997 Thermal rate constants of the O_2+N→ NO+O reaction based on the $^2A'$ and $^4A'$ potential-energy surfaces *J. Chem. Phys.* **107**, 6136–6145.

Gurvich, L.V., Veits, I.V. & Alcock, C.B. 1989 Thermodynamic properties of individual substances, volume 1: O, H/D,T/, F, Cl, Br, I, He, Ne, Ar, Kr, Xe, Rn, S, N, P, and their compounds, Part one: methods and computation, Part two: tables *New York, Hemisphere Publishing Corp., 1989.*

LeVeque, R. J. Balancing source terms and flux gradients in high-resolution Godunov methods: the quasi-steady wave-propagation algorithm, 1998 *J. Comp. Phys.* **146**, 346–365.

Magin, T. E., Caillault, L., Bourdon, A., & Laux, C. O. 2006 Nonequilibrium radiative heat flux modeling for the Huygens entry probe, *J. Geophys. Res.* **111**, E07S12.

Panesi, M., Magin, T. E., Bourdon, A., Bultel, A. & Chazot, O. 2009 Analysis of the FIRE II flight experiment by means of a collisional radiative model, *J. of Thermophysics and Heat Transfer* **23**, 236–248.

Park, C. 1993 Review of chemical-kinetic problems of future NASA missions. I - Earth entries *J. of Thermophysics and Heat Transfer* **7**, 385–398.

Park, C., Jaffe, R.L. & Partridge, H. 2001 Chemical-kinetic parameters of hyperbolic Earth entry *J. of Thermophysics and Heat Transfer* **15**, 76–90.

Sjögreen, B. & Yee, H. C. 2004 Multiresolution wavelet based adaptive numerical dissipation control for shock-turbulence computation, *RIACS Technical Report TR01.01, NASA Ames research center (Oct 2000); J. Sci. Comp.* **20**, 211–255.

Wang, W., Shu, C.-W., Yee, H. C.& Sjögreen, B. 2009 High order well-balanced schemes and applications to non-equilibrium flow, *J. Comp. Phys.*, **228**, 5787–5802.

Xing, Y. & Shu, C.-W. 2005 High order finite difference WENO schemes with the

exact conservation property for the shallow water equations, *J. Comp. Phys.* **208**, 206–227.

Xing, Y. & Shu, C.-W. 2006 High order well-balanced finite difference WENO schemes for a class of hyperbolic systems with source terms, *J. Sci. Comp.* **27**, 477–494.

Yee, H. C. 1989 A class of high-resolution explicit and implicit shock-capturing methods, *VKI lecture series 1989-04, March 6-10, 1989; NASA TM-101088, Feb. 1989.*

Yee, H. C. , Sandham, N. D., & Djomehri, M. J. 1999 Low dissipative high order shock-capturing methods using characteristic-based filters, *J. Comp. Phys.* **150**, 199–238.

Yee, H. C. & Sjögreen, B. 2007 Development of low dissipative high order filter schemes for multiscale Navier-Stokes/MHD systems, *J. Comp. Phys.* **68**, 151–179.

Yee, H. C., Sweby, P. K. & Griffiths, D. F. 1991 Dynamical approach study of spurious steady-state numerical solutions for non-linear differential equations, Part I: The dynamics of time discretizations and its implications for algorithm development in computational fluid dynamics, *J. Comp. Phys.* **97**, 249–310.